

DAMAGE DUE TO MICROCRACKING IN CEMENTITIOUS COMPOSITES USING AE FREQUENCY CHARACTERISTICS

NIKHIL GUPTA^{1*}, R. VIDYA SAGAR^{1†} AND J. M. CHANDRA KISHEN^{1‡}

¹Department of Civil Engineering,
Indian Institute of Science, Bangalore-560012, India.

*e-mail: nikhilgupta1@iisc.ac.in

†e-mail: rvsagar@iisc.ac.in

‡e-mail: chandrak@iisc.ac.in

Key words: Steel fiber reinforced concrete, Plain Concrete, Acoustic Emissions, Fast fourier transform, Microcracking, AE Frequency

Abstract. This study presents the transformation of acoustic emission (AE) waveforms from time domain to frequency domain using fast fourier transform (FFT) to understand the mechanisms underlying the fracture of cementitious composites. The motivation of the study is to introduce a real-time monitoring method based on frequency content of AE. The mode I fracture experiments are performed on plain concrete (PC) and steel fiber reinforced concrete (SFRC) in the laboratory. The fracture mechanisms of PC and SFRC are analyzed using the centroid of the frequency spectrum obtained from spectral analysis. The results indicate that there is no change in the frequency centroid spectrum (FCS) until the onset of microcracking in mode I crack deformation. After the microcracking begins, the slope of the FCS continuously decreases, indicating the rate of material damage over time. An accelerated crack growth denoted by slope of mean FCS is 2.7 times higher for PC when compared with SFRC. The slope of the mean FCS is nearly the same for both the initial and final regions of fracture mechanisms in PC. In SFRC, this rate is 29.2% lower due to fiber bridging mechanisms. A damage parameter, based on the FCS, is proposed to assess the damage and validated with the existing damage parameters. These observations suggests that FCS of AE waveforms may be used for real time damage monitoring of concrete structure.

1 INTRODUCTION

Cementitious composites, such as concrete, are widely used in the construction industry due to their cost-effectiveness, strength, and durability [1]. Recent advancements have focused on improving the mechanical properties of these composites. One notable innovation is the reinforcement of concrete with fibers, which significantly enhances the overall performance of the concrete [2]. However, susceptibility to damage caused by microcracking poses significant challenges to structural stability and long-term reliability. Microcracks can gradually degrade the

structural quality and increase vulnerability to deterioration [3]. Early detection and monitoring of these microcracks are crucial for effective maintenance, ensuring safety, and extending the lifespan of cementitious composites.

The acoustic emission (AE) testing has emerged as a powerful non-destructive testing (NDT) tool for monitoring microcracking in cementitious composites [4]. AE provides real-time insights into the fracture mechanisms of the material by detecting stress waves generated during the formation and propagation of cracks [5]. The frequency characteristics of AE

signals, such as peak frequencies and spectral distribution, provide essential data about the underlying damage mechanisms and the severity of microcracking. Recent advancements in signal processing and data interpretation have further enhanced the potential of AE techniques for precise damage assessment.

1.1 Literature Review

The analysis of AE signals involves studying various waveform parameters such as peak amplitude, duration, rise time, and frequency content. Among these, frequency characteristics specifically the peak frequencies and spectral distribution are particularly informative about the underlying damage mechanisms [6]. These characteristics are influenced by the inherent properties of material, type of damage, and the stage of crack propagation. High-frequency AE signals are often associated with crack initiation and propagation, while lower frequencies may indicate other forms of damage [7]. The peak frequency and spectral distribution of AE signals can be useful to differentiate between these damage mechanisms [8]. Recent advancements in signal processing techniques, such as empirical mode decomposition (EMD) and instantaneous dominant frequency (IDF) methods, have improved the analysis of AE signals [6]. EMD allows for the decomposition of complex AE signals into simpler intrinsic mode functions (IMFs), which can then be analyzed to extract meaningful frequency characteristics [8]. The IDF method, in particular, has shown promise in identifying critical damage by capturing the dominant frequency characteristics of AE signals.

Enhanced data interpretation methods, including machine learning algorithms and time-frequency analysis tools, have further improved the accuracy of AE based damage assessment [9]. Techniques such as short-time fourier transform (STFT) and wavelet transforms enable the detailed analysis of AE signals in both time and frequency domains, facilitating the identification of damage patterns and severity [10]. Similar to these methods, fast fourier

transform (FFT) algorithm is also used in literature to perform spectral analysis of AE waveforms [11]. The FFT algorithm is introduced in the literature, demonstrating that FFT is 100 times faster than the discrete fourier transform (DFT) for 2^{10} sample points [12]. Thus, FFT significantly enhances processing speed when handling large datasets, making it suitable for analyzing waveforms in the frequency domain. The results of FFT are utilized to perform feature analysis and recognition of fiber breakage across different types of fibers [13]. The experimental findings indicate that low-frequency AE signals are generated by tensile fractures, whereas high-frequency signals are associated with shear fractures [6].

Microcracking is one of the most challenging forms of damage to detect because it often involves minute changes in the material structure that are not immediately visible [14]. AE signals associated with microcracking are characterized by higher-frequency emissions, which are sensitive to the size and distribution of microcracks. The correlation between microcrack propagation and AE frequency patterns has been studied extensively [15]. The frequency characteristics of AE signals in the early stages of microcrack formation are often associated with the rupture of bonds at the microstructural level, while later stages of damage correspond to larger-scale crack propagation [16]. Therefore, understanding the frequency spectrum of AE signals can provide insights into the severity of the damage and the stage of crack growth [16].

1.2 Aim of the study

Each AE waveform is generated by different fracture mechanisms, resulting in distinct characteristics. These characteristics provide extensive information about the fracture behavior. Thus, the present study focuses on analyzing the frequency characteristics of AE waveforms to monitor damage due to microcracking. The comparison of plain concrete (PC) and steel fiber reinforced concrete (SFRC) is performed by correlating AE waveforms with the evolution

of microcracking.

This article is organized as follows: section 2 presents the methodology for AE data acquisition and frequency analysis. Section 3 describes the experimental setup and materials used. Section 4 discusses the results and their implications for damage monitoring. Finally, section 5 concludes the study.

2 METHODOLOGY

The frequency content of AE waveforms is obtained by converting time domain signal to frequency domain by FFT. The FFT is an optimized algorithm to compute the DFT efficiently. Direct computation of the DFT needs $O(N^2)$ operations for (N) data points, but the FFT reduces this to $O(N \log_2 N)$, significantly speeding up the process for large datasets [12]. The FFT of time domain sample points, $x(t)$ is computed by:

$$S(f_n) = \Delta t \sum_{k=0}^{N-1} x(t_k) e^{-j2\pi f_n t_k} \quad (1)$$

$$n = 0, \pm 1, \pm 2, \dots \pm \frac{N}{2}$$

$$\Delta t = \frac{T}{N}; \quad t_k = k\Delta t; \quad \Delta f = \frac{1}{T}; \quad f_n = n\Delta f$$

where, T is the total time a signal is observed in the time domain, and N is the number of sample points in the time domain. $x(t)$ and $S(f)$ represent the sample point of time and frequency domain, respectively. The visual representation of the algorithm is shown in Figure 1. Figure 1(a) depicts the time domain waveform obtained from AE testing, while Figure 1(b) illustrates the same signal after being converted into the frequency domain using FFT. In the analysis, only the first hit observed at any channel for each event is considered. This approach is considered to ensure consistency and avoid redundancy in the waveform data. The first hit is often the most significant and least affected by noise, usually showing the highest values of AE parameters.

The results are connected with the centroid of the frequency spectrum using the center of mass

formula to characterize the signal. The frequency centroid spectrum (FCS) is calculated as:

$$\text{FCS} = \frac{\sum_i f_i A(f_i)}{\sum_i A(f_i)} \quad (2)$$

where, $A(f_i)$ is the amplitude and f_i is the frequency of the i^{th} data point of waveform in frequency domain. Equation 2 shows a representative quantity of all the frequencies present in the frequency domain. The red dot in Figure 1(b) shows FCS computed for the waveform obtained at time of experiment 115.3 s.

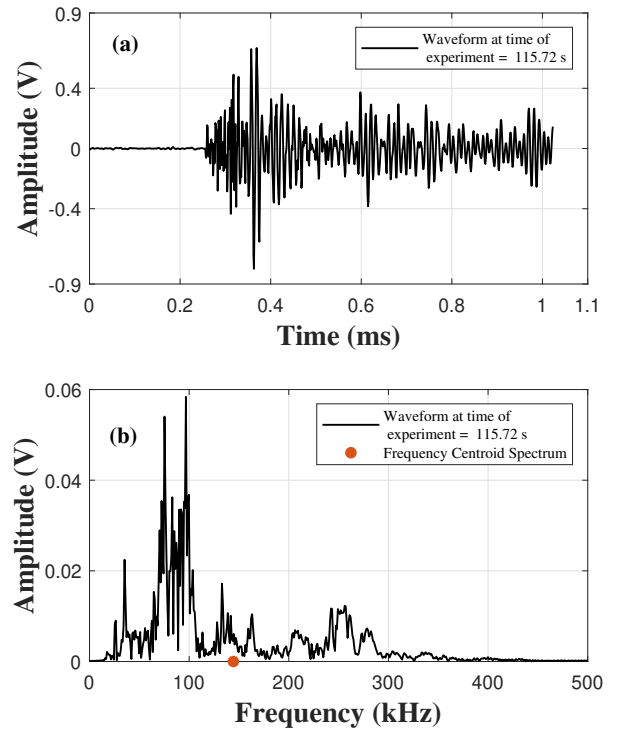


Figure 1: (a) Variation of time domain waveform at time 115.3 s; (b) Variation of frequency domain waveform at 115.3 s.

The damage is determined from the peak amplitude of AE waveforms [17]. The damage represents the degree of deterioration a cementitious material shows at that specific time. The

damage obtained using peak amplitude is calculated as:

$$\kappa = \sum_i 10^{3m_i} \quad (3)$$

Equation 3 shows κ , the damage parameter based on peak amplitude, where m_i represents the amplitude of hits in dB/20. The parameter κ is normalized using its final value. Further, a damage parameter (D) based on FCS is introduced in Equation 4. The damage assessed using FCS is compared with the damage determined from the peak amplitude of AE waveforms.

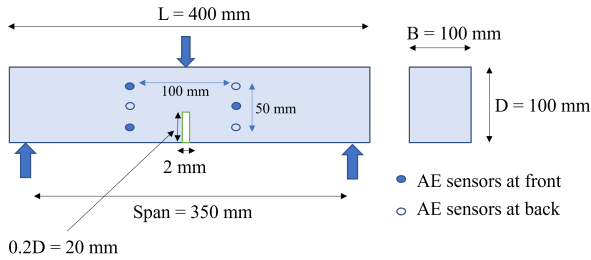


Figure 2: Geometric dimensions of notched three point bend specimen.

3 EXPERIMENTAL PROGRAM

The experimental program is presented in following sections:

3.1 Materials used and sample preparation

A set of five notched beams, each made of plain concrete (PC) and steel fiber reinforced concrete (SFRC), with dimensions shown in Figure 2, are prepared for testing. The mixture details of all the specimens are mentioned in Table 1. Ordinary Portland cement is used along with maximum coarse aggregate size of 10 mm and river sand as fine aggregate. Two-end hooked steel fibers, with a diameter of 0.5 mm, a length of 30 mm, and a tensile strength of 1269 MPa, are used.

3.2 Test setup

A CMOD-controlled three-point bending fracture test are performed using quasistatic monotonic loading. A 500 kN capacity servo-controlled hydraulic frame is used for testing,

with a loading rate of 0.0008 mm/s until 0.01 mm CMOD, and then 0.003 mm/s until the end of the test [as per EN: 14651:2005].

Table 1: Cementitious mixture details

Mix	Proportion	w/c	V_f (%)
PC	1:1.75:2.91	0.47	0
SFRC	1:1.75:2.91	0.47	1.5

V_f (%) :Volume fraction of fiber by weight; w/c: water to cement ratio by weight; Proportion: ratio of cement: fine aggregate: coarse aggregate by weight

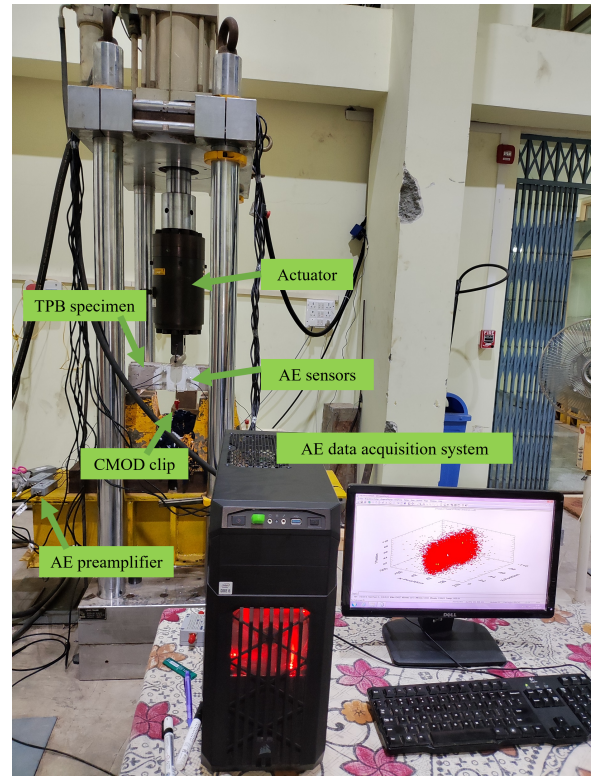


Figure 3: Experimental setup in Structures Laboratory, Department of Civil Engineering, Indian Institute of Science, Bangalore, India.

The generated AE waves are recorded using six piezoelectric sensors (PZT) mounted on the surface of the beam as shown in Figure 2 to conduct three dimensional (3D) source localization. The AE setup includes AE sensors, pre-amplifiers and AE data acquisition system. The R6 α PZT sensors having 54 kHz resonance frequency and manufactured by Physical Acoustic

Corporation (PAC) are used. The gain of pre-amplifiers and detection threshold is set to 40 dB. The experimental setup is shown in Figure 3.

4 RESULTS AND DISCUSSION

The mode I fracture experiments conducted on PC and SFRC show significant differences in the fracture behaviors. PC exhibits a quasi-brittle fracture with low fracture energy. Cracks in plain concrete propagate quickly, leading to rapid failure as shown in Figure 4. However, SFRC shows much higher fracture energy due to the presence of steel fibers, which bridge the cracks and enhance the toughness. The fibers slow down crack propagation by distributing stress components evenly, resulting in a gradual failure.

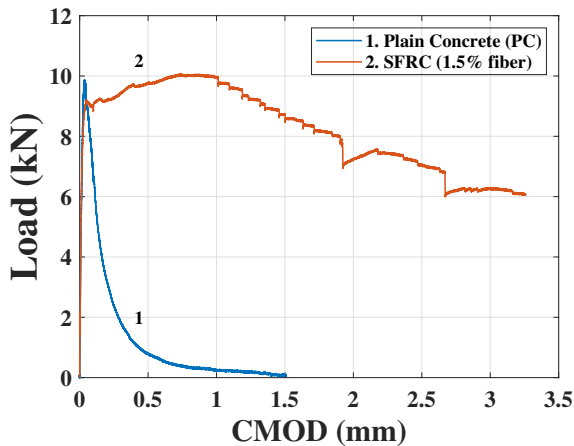


Figure 4: Variation of load with CMOD for PC and SFRC with 1.5% volume fraction of fiber under notched three point bend test.

The spectral analysis of all the AE waveforms recorded is computed using FFT algorithm. The FFT of one of the waveforms observed at 115.3 s is shown in Figure 1 to illustrate the frequencies present in the waveform. The FCS of the spectrum is calculated using Equation 2 and the variation is shown in Figure 5. To understand the change in FCS, the plot is divided into three potential regions, namely A, B, and C based on the damage levels [18]. In PC, region A corresponds to the time during

which the load remains above $0.8P_{max}$. Region B represents the time during which the load drops from $0.8P_{max}$ to $0.5P_{max}$ in the post-peak region. Region C is the time following region B. Similarly, for SFRC, region A starts at $0.8P_{max}$ in the pre-peak region and ends when the load begins to show hardening behavior. Region B ends when the load starts to soften after reaching the ultimate peak load.

4.1 Frequency characteristics of AE waveforms

In each region, the rate of change of FCS is observed by quantifying the slope (θ) of the mean FCS. The slope is calculated by linear regression and shown in Table 2. The experiments are conducted on five beams each of PC and SFRC under identical conditions. Due to the inherent heterogeneity of concrete, variability is expected. However, the results consistently exhibited the similar trend across all beams. Therefore, the results presented are representative of each cementitious composite composition.

Table 2: Rate of change of mean FCS in different region of mechanical behavior

Type of Material	Slope		
	θ_A	θ_B	θ_C
PC	-0.0380	-0.1026	-0.0329
SFRC	-0.0986	-0.0071	-0.0195

It is observed that at the start of region A, where microcracks begin to form, the FCS reaches its maximum value as shown in Figure 5. The mean value of FCS decreases in subsequent regions as various fracture mechanisms, such as microcrack initiation, coalescence, and macrocrack formation, occur. The slope of the decrement in mean FCS can be directly correlated with these mechanisms. In PC, the slopes of region A and region C are almost the same, suggesting slow crack propagation due to microcrack initiation in region A and macrocrack formation in region C. In region B, the coalescence of microcracks and macrocracks occurs,

accelerating the fracture process. This is indicated by the slope in this region, which is 2.7 times higher compared to other two regions.

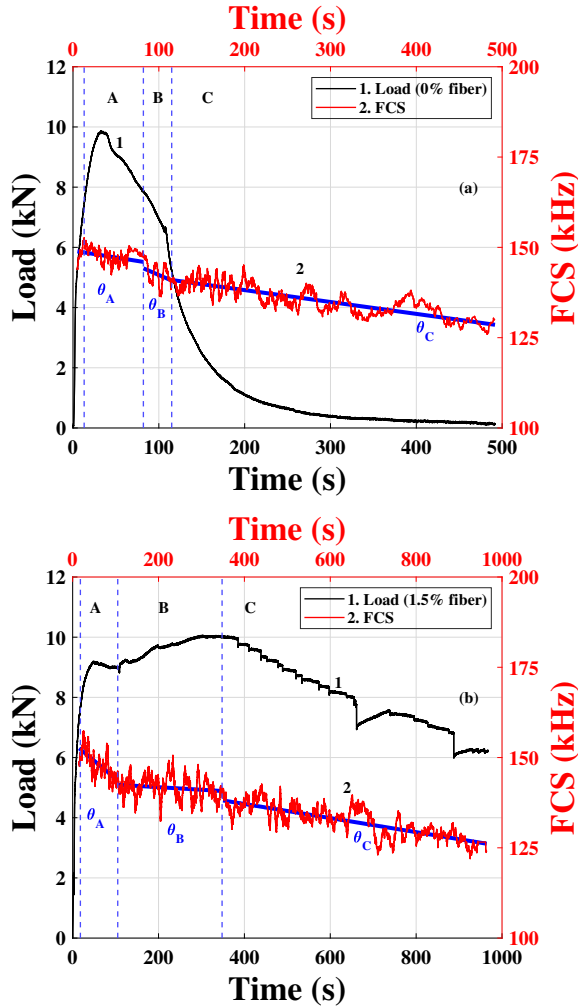


Figure 5: Variation of load and FCS with time for (a) PC, (b) SFRC with 1.5% volume fraction of fibers.

In SFRC, region B is the strain hardening region where load transfer from the cementitious matrix to steel fibers and reaches ultimate peak. This mechanism is reflected in the slope, θ_B . After an initial slope (θ_A), the slope (θ_B) remains almost constant, indicating the strengthening of the composite due to the fibers. In comparison with PC, in SFRC, the slope (θ_C) is not same as slope (θ_A). The softening behavior of concrete begins when sliding of fiber within the cement matrix occurs. The load gradually starts to transfer back to the matrix. How-

ever, due to fiber bridging, this process is delayed and occurs gradually. The slope change in FCS significantly correlates with the mechanism, showing a recovery of only 63.58% and a loss of 29.2% in the slope (θ_C) due to fiber mechanisms in region C. Hence, frequency content of AE waveforms is able to differentiate the regions and the mechanisms occurring in the cementitious composites.

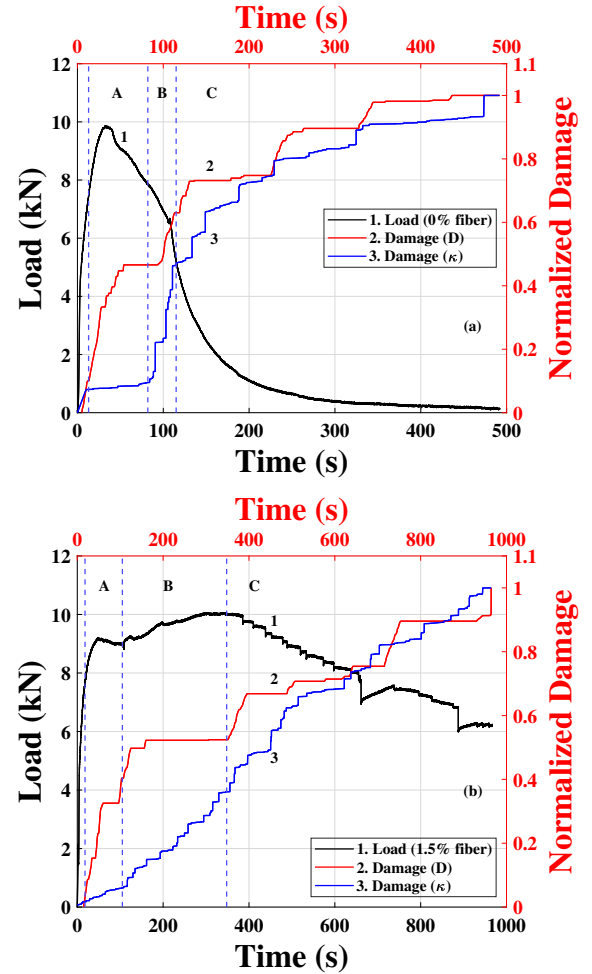


Figure 6: Variation of load and damage with time for (a) PC, (b) SFRC with 1.5% volume fraction of fibers.

4.2 Damage quantification based on frequency content of AE waveforms

Based on the results observed in the previous section, a damage parameter (D) based on FCS is introduced as:

$$D_i = \frac{FCS_{max} - FCS_i}{FCS_{max} - FCS_{last}} \quad (4)$$

where, FCS_{max} is the maximum value of FCS, FCS_i is the FCS value at i^{th} time, and FCS_{last} is last value of FCS observed in the experiment. To avoid fluctuations ‘ D ’ cumulative maximum value is considered. Along with this, the damage (κ) presented in Equation 3 is plotted for comparison in Figure 6.

It can be observed that damage starts at the beginning of region A. However, the damage parameter shows a slightly higher value than ‘ κ ’ which is validated [19]. The inefficiency of κ in capturing this damage may be due to the formation of microcracks in the region, which release AE waveforms with very low peak amplitudes. In PC, the trend of both damage parameters exhibits the same behavior, effectively indicating the increase in damage due to crack coalescence in region B. However, in SFRC, the damage parameter shows that damage does not progress until the strain hardening region is completed. After this region, both damage parameters nearly coincide.

5 CONCLUSIONS

The study presents the analysis of the AE waveforms generated during mode I fracture. The frequency characteristics are studied using FFT to understand the damage occurring in the cementitious composites. The following major conclusions are drawn:

1. The FCS reaches its maximum value at the time when microcracking starts in the cementitious composites.
2. The decay in value of FCS is observed as the fracture progresses.
3. The slope change of mean FCS can be correlated with the fracture mechanisms occurring in the composites.
4. The slope of the mean FCS is nearly the same for both the initial and final regions of fracture mechanisms in PC. In SFRC, the slope is 29.2% lower due to fiber bridging mechanisms.

5. The damage based on FCS can be used to predict failure. Hence, serves as an indicator to estimate the remaining life of a structure.

REFERENCES

- [1] Jan G.M. van Mier. *Concrete Fracture: A Multiscale Approach*. CRC Press, October 2012.
- [2] Nagesh R. Iyer. *An overview of cementitious construction materials*, page 1–64. Elsevier, 2020.
- [3] Corina-Maria Aldea, Surendra P. Shah, and Alan Karr. Effect of microcracking on durability of high-strength concrete. *Transportation Research Record: Journal of the Transportation Research Board*, 1668(1):86–90, January 1999.
- [4] Masayasu Ohtsu, Toshiro Isoda, and Yuichi Tomoda. Acoustic emission techniques standardized for concrete structures. *Journal of Acoustic Emission*, 25(2007):21–32, 2007.
- [5] Nikhil Gupta, R Vidya Sagar, and J.M. Chandra Kishen. Time function analysis of acoustic emissions generated during compressive fracture process in steel fiber reinforced concrete. In *proceedings of the 11th International Conference on Fracture Mechanics of Concrete and Concrete Structures, Bangalore, India, FraMCoS-11*. IA-FraMCoS, September 2023.
- [6] Ruochen Jiang, Feng Dai, Yi Liu, Ang Li, and Peng Feng. Frequency characteristics of acoustic emissions induced by crack propagation in rock tensile fracture. *Rock Mechanics and Rock Engineering*, 54(4):2053–2065, February 2021.
- [7] Meilin Zhang, Qinghui Zhang, Junqiu Li, Jiale Xu, and Jiawen Zheng. Classification of acoustic emission signals in wood damage and fracture process based on empirical mode decomposition, discrete wavelet

- transform methods, and selected features. *Journal of Wood Science*, 67(1), October 2021.
- [8] Aijun Gu, Zefeng Liu, Rui Pan, and Bo Xu. Damage identification in concrete using instantaneous dominant frequency of acoustic emission signals. *Buildings*, 14(12):3784, November 2024.
- [9] Primož Potočnik, Martin Misson, Roman Šturm, Edvard Govekar, and Tomaž Kek. Deep feature extraction based on ae signals for the characterization of loaded carbon fiber epoxy and glass fiber epoxy composites. *Applied Sciences*, 12(4):1867, February 2022.
- [10] Mohamed Barbosh, Kyle Dunphy, and Ayan Sadhu. Acoustic emission-based damage localization using wavelet-assisted deep learning. *Journal of Infrastructure Preservation and Resilience*, 3(1), April 2022.
- [11] D Masera, P Bocca, and A Grazzini. Frequency analysis of acoustic emission signal to monitor damage evolution in masonry structures. *Journal of Physics: Conference Series*, 305:012134, July 2011.
- [12] E. O. Brigham and R. E. Morrow. The fast fourier transform. *IEEE Spectrum*, 4(12):63–70, December 1967.
- [13] Xuejiao Chen, Xiaoyan Tong, Leijiang Yao, and Bin Li. Feature analysis and recognition of fiber breakage ae signals after propagation. *AIP Advances*, 14(8), August 2024.
- [14] Caiyuan Fan, Jinfeng Liu, and Fanbao Meng. Microcracking process characterization and failure time prediction of three typical rocks upon uniaxial compression based on acoustic emission activity. *Rock Mechanics and Rock Engineering*, 57(11):9145–9164, July 2024.
- [15] Kui Zhao, Daoxue Yang, Cong Gong, Yulong Zhuo, Xiaojun Wang, and Wen Zhong. Evaluation of internal microcrack evolution in red sandstone based on time–frequency domain characteristics of acoustic emission signals. *Construction and Building Materials*, 260:120435, November 2020.
- [16] Christian U Grosse, Masayasu Ohtsu, Dimitrios G Aggelis, and Tomoki Shiotani. *Acoustic emission testing: Basics for research–applications in engineering*. Springer Nature, 2021.
- [17] S.J.D. Cox and P.G. Meredith. Microcrack formation and material softening in rock measured by monitoring acoustic emissions. *International Journal of Rock Mechanics and Mining Sciences & Geomechanics Abstracts*, 30(1):11–24, February 1993.
- [18] Nazirah Mohd Apandi, Chau-Khun Ma, Chee-Loong Chin, Abdullah Zawawi Awang, Wahid Omar, Ahmad Safuan A. Rashid, and Warid Wazien Ahmad Zailani. Preliminary pre-damaged level assessment for concrete structures: A review. *Structures*, 54:1381–1390, August 2023.
- [19] Tohid Asheghi Mehmandari, Mehdi Shokouhian, Mohammad Zakeri Josheghan, Seyed Ali Mirjafari, Ahmad Fahimifar, Danial Jahed Armaghani, and Kong Fah Tee. Flexural properties of fiber-reinforced concrete using hybrid recycled steel fibers and manufactured steel fibers. *Journal of Building Engineering*, 98:111069, December 2024.